

Star Formation in the Circumnuclear Environment of NGC 1068

Richard I. Davies,^{1*} Hajime Sugai² and Martin J. Ward³

¹ *Astrophysics, Oxford University, Nuclear Physics Building, Keble Road, Oxford, OX1 3RH, UK*

² *Department of Astronomy, Kyoto University, Kyoto 606-01, Japan*

³ *Department of Physics and Astronomy, Leicester University, Leicester, LE1 7RH, UK*

Accepted 1988 December 15. Received 1988 December 14; in original form 1988 October 11

ABSTRACT

We present near-infrared emission line images of the circumnuclear ring in NGC 1068. We have measured the Br γ fluxes in a number of star forming complexes and derived extinctions for each of these by comparison with H α . We investigate the star forming histories of these regions and find that a short burst of star formation occurred co-evally throughout the ring within the last 30–40 Myr, and perhaps as recently as 4–7 Myr ago. The 1-0 S(1) flux and S(1)/Br γ ratios indicate that as well as fluorescence, shock excited H₂ emission contributes to the total flux. There is excess H₂ flux to the North-West where the ionisation cone crosses the ring, and we have shown it is possible that the non-stellar continuum from the Seyfert nucleus which produces the high excitation lines could also be causing fluorescence at the edges of molecular clouds in the ring. The nuclear 1-0 S(1) is more extended than previously realised but only along the bar's major axis, and we consider mechanisms for its excitation.

Key words: galaxies: individual: NGC 1068 – galaxies: Seyfert – galaxies: starburst – infrared: galaxies.

1 INTRODUCTION

NGC 1068 is considered an archetypal Seyfert 2 galaxy, and being nearby and bright (14.4 Mpc and $L_{\text{IR}} = 2 \times 10^{11} L_{\odot}$, Ringberg Standard) has been observed extensively. In recent years much effort has been devoted to studying the nucleus at ever higher spatial resolutions, exemplified by a direct 8.4 GHz image of the inner torus at a resolution of 2 milli-arcsec (Gallimore, Baum & O'Dea, 1997), and adaptive optics imaging (Thatte et al. 1997) which showed that 94 per cent of the K-band light in the central 1 arcsec originates from a ≤ 30 milli-arcsec source, the remainder being due to a nuclear star cluster.

But the circumnuclear ring at a radius of 15–16 arcsec should not be overlooked as here the H II regions, equivalent to a string of M 82-type galaxies, rival the nucleus in terms of bolometric luminosity. Tesco & Decher (1988) explained the ring in terms of inner Lindblad resonances associated with a barred potential, and Scoville et al. (1988) showed that there was also a bar extending from this ring closer in towards the nucleus. Such a hierarchical structure is one of the most efficient ways in which to transport gas over the 3–

4 orders of magnitude in scale from the disk, not only into the circumnuclear regions, but into the nucleus itself. Understanding what processes are operating in the ring, and how and why they do so is a necessary step towards a global picture of NGC 1068. Atherton, Reay & Taylor (1985) presented a velocity resolved H α image of the ring and circumnuclear environment, finding that there were a large number of clouds with highly turbulent motions, and possibly a large scale expansion of the disc. This expansion was also seen by Planesas, Scoville & Myers (1991) who made high resolution CO observations. The CO observations revealed a large number of cloud complexes in the ring and nucleus, which appear to be much warmer (~ 50 K) and more massive (up to several $\times 10^8 M_{\odot}$) than molecular clouds in the Galaxy.

The inner disk has one of the highest blue surface brightnesses known (Keel & Weedman, 1978) and is the origin for about 1/3 as much H α again as the ring. Bland-Hawthorn, Sokolowski & Cecil (1991) argue that this diffuse ionised medium, characterised by a high [N II]/H α ratio, is excited by scattered nuclear radiation, whereas the high excitation lines (Evans & Dopita 1986; Bergeron 1989) arise in gas which has a direct line of sight to the Seyfert nucleus. The morphology of the high excitation gas has been studied in detail by Pogge (1988) and Unger et al. (1992), who traced it out beyond the ring at PA 11–51°. An ionisation cone such as this would naturally occur as a direct

* Current address: Max-Planck-Institut für extraterrestrische Physik, Postfach 1603, 85740 Garching, Germany
email: davies@mpe.mpg.de

result of collimation by a molecular torus, but simple interpretation of the observations in terms of this model is not possible. Unger et al. demonstrate that a proper analysis requires careful study of the complex geometries of the radio jet, [O III] cone, UV field, etc.

Because of its brightness, proximity and favourable orientation, NGC 1068 provides an excellent laboratory for studying the Seyfert nucleus, inner disk and circumnuclear ring. Such work in many different wavebands (see the collage in Bland-Hawthorn et al. 1997) is already providing insights into how these phenomena are inter-linked, a topic which is receiving considerable attention at present. One aspect which has been previously omitted is the circumnuclear near-infrared line emission and in this paper we present the first such 1-0S(1) and Br γ images, which have been made possible because of the wide field available with the Fabry-Perot and IRCAM3 on UKIRT. We study individual star forming complexes, and by comparison of the recombination line strengths determine the extinctions to each region. We look at the timescales for the star formation, determining whether it is co-eval throughout the ring and if there have been previous episodes of activity in Section 5. In Section 6 we consider triggering mechanisms with reference the effect of the ionisation cone and radio jet, and in Section 7 we discuss the origin of the 1-0S(1) emission in the ring. Our signal-to-noise is sufficient to have revealed H₂ emission near the nucleus which is more extended than was previously realised, and in Section 8 we consider what may be the cause of this. We summarise our conclusions in Section 9.

2 OBSERVATIONS AND DATA REDUCTION

Images of the 2 μ m continuum, and H₂ 1-0S(1) and Br γ emission lines were obtained with the UKIRT 3.8-m telescope on the nights of 19 and 20 December 1996, using the tip-tilt facility. A Fabry-Perot etalon, with spectral resolution of 325 km s⁻¹, was used in conjunction with IRCAM3 at the Cassegrain focus. IRCAM3 is a near-infrared camera housing a 256 \times 256 InSb array with a scale of 0.3 arcsec per pixel, giving an unvignetted field of view of more than 60 arcsec. Cooled narrow band filters (FWHM 2.4 per cent) were used for order sorting, and wavelength calibration was achieved by peaking up on the 2.1171 μ m line from a Krypton lamp.

The observations were carried out as follows. For each line, 2 or 3 minute observations of the object were made at the on-line wavelength and also of the continuum at slightly shorter and longer wavelengths (shifted with respect to the line centre by ± 1200 km s⁻¹ for 1-0S(1), and by $-1200, +1080$ km s⁻¹ for Br γ). Sky frames were also made at each wavelength. This was repeated until sufficient on-line integration had been achieved.

IRAF was used for all the image processing and analysis as described below. A flatfield was made from the bias-subtracted 3-minute sky-frames. This was then divided into the object frames after each corresponding sky frame had been subtracted. Frames were registered on the bright peak of emission from the Seyfert nucleus. Each frame was then flux calibrated. Non-photometric conditions on the first night and saturation of the star used for Br γ , meant that only the 1-0S(1) line on the second night could be calibrated

directly from a standard star (HR 1091, an A1 star with no spectral features at the wavelengths used). All the other frames were self-calibrated; that is, the continuum (sampled only in regions with no line emission) was scaled to match the calibrated frames. This was feasible because the continuum emission in NGC 1068 is bright over a sufficiently extended area.

Multiple ghost images were a severe problem with this object. However, as the location of the ghosts was different for the two nights on which the observations were made, these could be masked out. This was carried out while co-adding the individual calibrated frames. Finally, the continuum frame was subtracted from the on-line frames to leave ghost-free line-only images. The total on-line integration times were 42 minutes for Br γ and 30 minutes for 1-0S(1).

The resolution (including the effects of seeing and registering, as well as the enhancement afforded by the tip-tilt) was measured from the standard star profiles to be 1.0 arcsec. Unfortunately, as the emission is extremely faint, the images in Figure 1 have had to be smoothed with a median filter to enhance the signal-to-noise, reducing the resolution to either 1.4 or 1.7 arcsec as shown.

2.1 Calibration & the Velocity Field

One important point to consider is whether the calibration is significantly affected by the velocity distribution of the line emitting gas itself, since Atherton et al. (1985) showed that the line-of-sight velocities of H α in the circumnuclear ring varied over 1020–1260 km s⁻¹. For our observations we centred the FP at 1136 km s⁻¹, corresponding to a heliocentric velocity of 1114 km s⁻¹, so that the 325 km s⁻¹ resolution of the FP covered the range 950–1280 km s⁻¹. However, there is a shift in transmitted wavelength (towards shorter wavelengths) which increases to larger radius, reaching $\delta\lambda \equiv 160$ km s⁻¹ at $r = 30$ arcsec. Since $\delta\lambda \propto r^2$, we estimate that in the ring $\delta\lambda \equiv 40$ km s⁻¹. We have taken this into account when correcting fluxes for the variations in velocity. The correction required has been calculated as $1/A(v)$ where $A(v)$ is the value of the Airy function at a velocity v offset from peak transmission. The velocity dispersion of the lines has not been included since it would require detailed knowledge of the line profiles across the entire field, and would only entail an additional correction varying from almost zero to a maximum of 10 per cent in the South-West where $\sigma > 135$ km s⁻¹.

The approximate velocities of the Br γ components marked in Fig. 1 are given in Table 1, together with the correction factor. Throughout the rest of the paper, the observed fluxes given have been velocity corrected. The whole image has not been corrected as, instead of simplifying its interpretation, it would serve only to introduce a variable detection limit across the field.

3 NEAR-INFRARED LINE MORPHOLOGY

Images of the Br γ and 1-0S(1) line emission, and 2 μ m continuum are presented in Figure 1. The central regions have not been contoured; instead the location of the nucleus, as

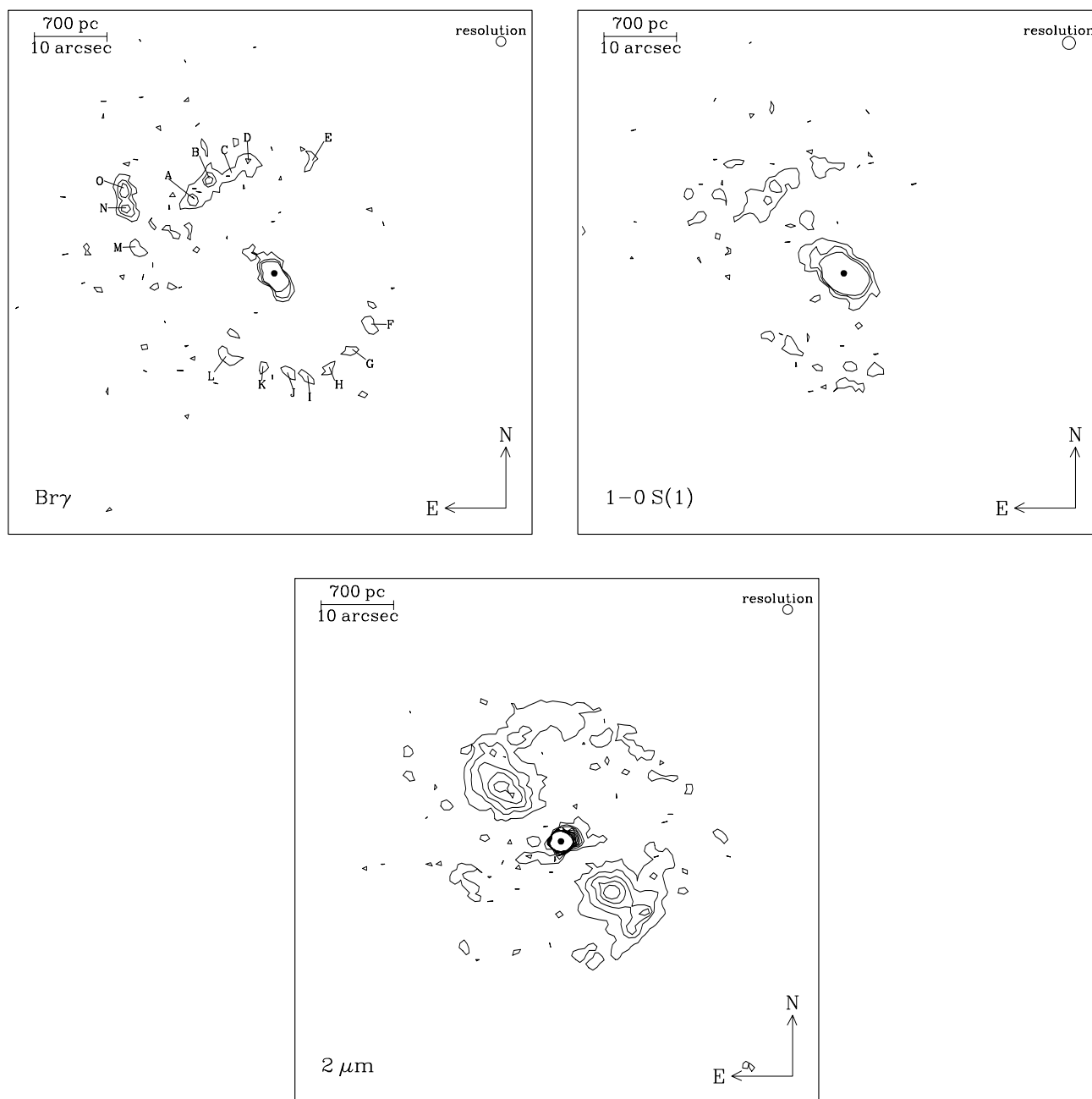


Figure 1. Contour plots of a $72 \times 72 \text{ arcsec}^2$ field at the centre of NGC 1068. The calibration shown in the line images has not been corrected for the velocity field. Upper Left – $\text{Br}\gamma$ line emission, with contours at 2.9 , 5.7 & $8.6 \times 10^{-19} \text{ W m}^{-2} \text{ arcsec}^{-2}$; the lowest contour is 2.5σ . Upper right – $1-0\text{S}(1)$ line emission, with contours at the same intervals; the lowest contour is 3σ due to the greater smoothing used. Lower – $2 \mu\text{m}$ continuum after subtraction of best-fit ellipses, with contours from 0.1 – $2.3 \text{ mJy arcsec}^{-2}$ at intervals of $0.2 \text{ mJy arcsec}^{-2}$; the lowest contour is 2.5σ . The central (peak) region has not been contoured and instead the location of the nucleus is marked by a large dot.

defined by the centroid of the continuum emission, has been marked with a large dot.

3.1 $2 \mu\text{m}$ continuum

Calibration of the continuum in several annuli compares favourably to that in Scoville et al. (1988). The emission is dominated by elliptical isophotes, and in order to better recover the fainter underlying structure, these have been mod-

elled and subtracted using tasks in the ISOPHOTE package within IRAF. In order to preserve this structure, its inclusion in the fitting process was avoided by using a clipping algorithm which removed the 40 per cent of pixels with the highest counts before fitting each isophote. The bar is very clear lying along position angle 46° , as has been measured by other authors (eg Scoville et al. 1988). At the regions of peak intensity in the residual image, the bar has a surface brightness approximately 75 per cent of the underlying ellip-

Table 1. Flux Correction Factors

Region	Position (arcsec from nucleus)		Velocity km s ⁻¹	Correction factor
A	11.4 E	10.2 N	1050	1.01
B	9.1 E	12.9 N	1090	1.02
C	6.0 E	13.6 N	1120	1.11
D	3.7 E	15.3 N	1130	1.16
E	5.2 W	15.3 N	1220	1.90
F	13.2 W	7.2 S	1270	2.57
G	10.6 W	10.7 S	1260	2.41
H	7.4 W	13.1 S	1200	1.68
I	4.5 W	14.3 S	1180	1.49
J	1.7 W	13.3 S	1160	1.33
K	1.7 E	13.0 S	1140	1.21
L	6.8 E	11.6 S	1060	1.00
M	19.2 E	3.4 N	1010	1.12
N	20.5 E	9.0 N	1030	1.05
O	20.8 E	12.1 N	1030	1.05

tical isophotes. Closer to the nucleus, the clipping algorithm may not have been efficient in excluding pixels in the bar due to the small size of the ellipses and width of the bar. We therefore do not consider the apparent lack of structure close to the nucleus to be significant; indeed the H₂ emission suggests that the bar does continue much further in (see also Section 8). All the remaining structure in the residual image, particularly at the southern end of the bar and the spiral arm west of the northern end of the bar, also appears in the original continuum image.

It is interesting that the strongest continuum in the ring follows the 10 μm morphology rather than that indicated by Hα or Brγ knots, suggesting that the emission mechanisms may be associated.

3.2 Molecular Hydrogen 1-0S(1)

The 1-0S(1) emission is relatively strong at the end of the bar to the North-East, as well as projecting from the nucleus along the first few arcsecs of the bar. The morphology in the central few arcsecs is consistent with that observed by Rotaciuc et al. (1991) and Blietz et al. (1994). The nuclear region shows a strong peak almost due East of the nucleus and a weaker one to the South-West (Fig. 4), but these authors did not observe the more extended nuclear emission as their data went less deep. As a rough consistency check of the total flux in a 6 × 6 arcsec² aperture, we first interpolated across the pixels badly affected by the saturation, and then applied a 20 per cent correction for the 200 km s⁻¹ line width. The resulting flux of $13.8 \pm 0.1 \times 10^{-17}$ W m⁻² agrees well with that measured by Oliva & Moorwood (1990) in a similar aperture, and also Blitz et al. (1994).

Reay, Atherton, and Walton (1986) previously detected 1-0S(1) at two points in the ring using a spectrometer with a 5.4 arcsec aperture. At the North-East end of the bar they measured an intensity almost an order of magnitude greater than ourselves. We believe that large error bars (points on the spectrum are 2–3σ above their continuum level) combined with an underestimate of the continuum level, have led to an overestimate of the line flux. Their nuclear flux,

detected at a much higher signal-to-noise, is consistent with our measurement.

3.3 Hydrogen Recombination Brγ

The Brγ clearly delineates sections of the circumnuclear ring, showing distinct similarities to that seen in the Hα line map (Bland-Hawthorn, Sokolowski & Cecil, 1991). Although the strongest emission appears to be to the North-East, this is partly due to the effects of the velocity field as described in Section 2.1. Table 2 shows that the emission to the South-West is as strong as that in the North-East section of the ring. The relative apparent weakness of the emission to the West is also due to velocity effects, with the result that any Brγ emission is below our detection threshold. In the nucleus there is evidence for a single strong peak, as observed by Rotaciuc et al. (1991).

4 EXTINCTION

The extinction towards individual H II regions may not be uniform. Young, Kleinmann & Allen (1988) mapped the extinction using the ratio of [S III] λ9532Å to (Hα + [N II]). They found that it peaked at $A_V = 1.5$ mags to the North-East, and at $A_V = 2.5$ mags to the South-West. However, the assumption made in order to produce these maps has been questioned by Kennicutt & Pogge (1990) who found an order of magnitude scatter in the intrinsic [S III]/Hα ratio in H II regions. They suggested that variations in the observed ratio might reflect variations in the level of gas excitation rather than dust extinction, and in the circumnuclear regions of NGC 1068 several different line excitation processes may be operating, including photoionisation from the nucleus and possibly relativistic electrons associated with the nuclear jet (Cecil, Bland & Tully 1990).

We have therefore measured the extinction in different regions by comparing our Brγ image to an Hα image kindly provided by J. Bland-Hawthorn (Bland-Hawthorn et al. 1991). This image shows *pure* Hα emission, as the contribution from [N II] has been mapped and subtracted by fitting spectra at each pixel. The image was calibrated by fixing the total line flux to be that determined previously by these authors, 4.6×10^{34} W m⁻². This was further verified by determining the difference in (Hα + [N II]) flux (taking the average ratio $H\alpha / (H\alpha + [N II]) = 0.5$) between a 13.5 arcsec aperture (McQuade, Calzetti & Kinney, 1995) and a 64 arcsec aperture (Young et al. 1988). These agreed to within 9 per cent. The Brγ image was smoothed to a similar resolution (approximately 3 arcsec FWHM) and re-binned to a scale of 0.5 arcsec pixel⁻¹ to match the Hα image. The images were then registered with reference to several prominent H II regions in the ring. Brγ and Hα fluxes were measured in the regions A–O using 3 arcsec apertures. The Brγ fluxes were then velocity corrected as described in Section 2.1 before deriving the extinction. This was done assuming an intrinsic ratio $H\alpha / Br\gamma = 103.6$ (Osterbrock 1989) and using the Howarth (1983) galactic extinction curve. The results are given in Table 2.

Typical values are $A_V = 1–3$ mag similar to those found by Young et al. (1988), suggesting that reddening corrections to infrared line fluxes are relatively small. This result

is important because by using a diagnostic in the K-band we should be able to detect H II regions to optical depths much greater than an A_V of 3 mag since $\tau_{2.2\mu\text{m}} = 1$ at $A_V \simeq 9$ mag. The issue cannot be avoided by considering, instead of the usual ‘screen’ model, a ‘mixed’ model which allows one to infer significantly higher A_V but for which we still derive only $A_V = 3\text{--}17$ mag. It implies that in regions where we see star formation, either it is occurring only near the surface, or the molecular clouds are not highly optically thick. The latter option seems unlikely from CO observations which imply considerably higher optical thicknesses for the clouds, and the former appears to require some external influence on the star formation.

5 TIMESCALES FOR STAR FORMATION

The spatial resolution in Fig. 1 has allowed us to measure the FWHM of some Br γ knots as 1.3 arcsec (90 pc), and in the unsmoothed image we have measured the brightest knot to have a FWHM of 0.9 arcsec (60 pc). These upper limits to the cluster sizes, and the masses we derive in this section, suggest that each region A–O, if not an individual OB association, is probably a relatively small number of such associations.

We can determine the age of the star formation by measuring the equivalent width (EW) of the Br γ line in these clusters. In order to estimate the continuum flux density associated only with young stars we have subtracted the underlying isophotes (Fig. 1). Careful comparison of the images suggests the labelled regions even close to the bar will suffer little or no contamination from the continuum in the bar. The Br γ and continuum fluxes in 3 arcsec apertures at these sites are given in Table 2, and show that $\text{EW}(\text{Br}\gamma) = 20\text{--}200\text{\AA}$. We use the evolutionary synthesis models of Leitherer & Heckman (1995) to determine the starburst history, making the assumptions of solar metallicity and a standard IMF (Salpeter in the range 1–100 M_\odot).

If the star formation is instantaneous (i.e., the duration is small compared to the time elapsed since it occurred) then around the whole ring, it occurred from 4–7 Myr ago. The similarity in the ages even with an order of magnitude difference in EW is due to the very rapid decrease in EW with time, reflecting the speed of evolution of the most massive stars away from the main sequence. The ionising flux N_{UV} is derived from the dereddened Br γ flux making the usual assumption that 70 Lyman continuum photons are required for each Br γ photon produced. This and the age can then be used to determine the mass of stars formed in each region, which is $10^5\text{--}10^6 M_\odot$.

Alternatively, if the star formation is still progressing, then the ages range from 6 Myr to more than 300 Myr (unless the IMF is truncated). Although the total mass of stars formed would be of the order of $10^6\text{--}10^7 M_\odot$ in each complex, this is still several times smaller than the available gas mass (estimated from the CO luminosity, Planesas et al. 1991) and so does not rule out the scenario. We believe that continuous star formation is unlikely as it would need to be sustained over timescales of more than 100 Myr in highly specific regions. In a single star cluster, once massive young stars have formed, the turbulence and heating from these would begin to disrupt the remainder of the giant molecular cloud

(GMC) and inhibit further star formation. After a few million years these stars would evolve to produce supernovae, injecting more kinetic energy into the local ISM. Further star formation would be halted after only a few generations of OB stars. Blitz & Shu (1980) and Blitz (1991) used observational and theoretical evidence to argue that GMCs which generate OB associations cannot have lifetimes much greater than 20–40 Myr. A simple persuasive line of reasoning concerns the gravitational binding energy of a GMC, typically 10^{50} erg for a $2 \times 10^5 M_\odot$ cloud of size 40 pc. By estimating the luminosity of OB stars formed over 10^7 yrs and the efficiency with which this could be converted into kinetic energy Blitz & Shu found that 10^{51} erg were available over this time, which could produce expansion speeds of $\sim 10 \text{ km s}^{-1}$ capable of dispersing the cloud. Thus even without considering the kinetic energy released by supernovae (typically 10^{51} erg for a type II supernova), the active star formation episode in GMCs is necessarily short lived. More detailed calculations of the mechanical energy deposited in the ISM are included in Leitherer & Heckman’s models and we apply these to NGC 1068. They show that for a cluster undergoing constant star formation with the typical Br γ luminosity observed, it exceeds the binding energy of $\sim 10^{55}$ erg for the larger molecular clouds (Planesas et al. 1991) after 30–40 Myr. This therefore provides an upper limit to the duration of the star forming episodes here. The masses of the clouds may actually be much less as there is some evidence that the CO-to-H $_2$ conversion factor has been overestimated, in which case the binding energy would be significantly smaller and the limit on the duration of star formation could be less than 10–20 Myr.

We conclude that the active phase in the ring is short-lived, these are young star clusters, and that the star formation is co-eval on a timescale of 10 Myr. The $2 \mu\text{m}$ continuum in these regions can be accounted for entirely by this star formation, so that we find no evidence for previous episodes of star formation. Since strong H α is observed around the whole ring, the arguments above can be extended to the regions where we could not detect Br γ . Even to the West where we observe continuum emission ($0.1 \text{ mJy arcsec}^{-2}$) but no Br γ ($< 0.22 \times 10^{-18} \text{ W m}^{-2} \text{ arcsec}^{-2}$ averaged over a 3 arcsec aperture and velocity corrected), the upper limit for $\text{EW}(\text{Br}\gamma)$ is 35\AA consistent with an age of 6 Myr. We therefore also conclude that this is probably the first episode of star formation in the ring.

6 TRIGGERING STAR FORMATION

The existence of the circumnuclear ring in NGC 1068 has been attributed to gas settling between the inner Lindblad resonances (ILRs) as a result of the action of a barred gravitational potential (Telesco & Decher 1988). In such situations we expect vigorous star formation to occur as a direct result of the increased cloud density at the ILR. The Schmidt Law describes the star formation rate as dependent on the local gas surface density ($SFR \propto \rho_{\text{gas}}^n$ with $1 < n < 2$, eg Kennicutt 1989) because the higher cloud density leads to an increased cloud collision rate so that GMCs are more likely to form and compression induced cloud collapse to occur, both of which will enhance the star formation rate. This appears to be substantiated, at least qualitatively, by

Table 2. Star Formation Properties

Region	A_V mag	Observed flux ^a $10^{-18} \text{ W m}^{-2}$		Corrected flux ^b $10^{-18} \text{ W m}^{-2}$		$2 \mu\text{m cont.}^c$ mJy	S(1)/Br γ ratio	EW (Br γ) Å	$\log N_{UV}$ 10^{51} s^{-1}	Age ^d Myr	Mass ^d $10^6 M_\odot$
		Br γ	1-0S(1)	Br γ	1-0S(1)						
A	1.2	3.3 ± 0.2	3.5 ± 0.3	3.7 ± 0.2	3.9 ± 0.3	3.24 ± 0.03	1.0 ± 0.1	16 ± 1.0	6.6	6.5	1.1
B	2.0	4.3 ± 0.2	3.2 ± 0.3	5.1 ± 0.3	3.9 ± 0.4	2.27 ± 0.03	0.8 ± 0.1	29 ± 1.5	9.1	6.1	1.1
C	1.9	2.7 ± 0.2	1.8 ± 0.3	3.2 ± 0.3	2.2 ± 0.4	1.98 ± 0.03	0.7 ± 0.1	21 ± 1.9	5.7	6.2	0.8
D	2.0	3.6 ± 0.2	2.3 ± 0.3	4.3 ± 0.3	2.7 ± 0.4	1.24 ± 0.03	0.6 ± 0.1	45 ± 3.3	7.6	5.8	0.8
E	3.2	3.4 ± 0.4	1.7 ± 0.5	4.6 ± 0.5	2.3 ± 0.7	0.65 ± 0.03	0.5 ± 0.2	83 ± 11	8.2	5.3	0.6
F	1.1	5.7 ± 0.5	< 2.2	6.4 ± 0.6	< 2.4	1.91 ± 0.03	< 0.4	47 ± 4.5	11.2	5.8	1.2
G	1.3	3.6 ± 0.5	< 2.1	4.1 ± 0.6	< 2.3	3.84 ± 0.03	< 0.6	15 ± 2.1	7.2	6.6	1.2
H	1.5	3.1 ± 0.4	< 1.4	3.6 ± 0.4	< 1.7	1.09 ± 0.03	< 0.5	45 ± 5.2	6.6	5.8	0.7
I	2.8	2.8 ± 0.3	1.6 ± 0.4	3.7 ± 0.4	2.1 ± 0.6	0.44 ± 0.03	0.6 ± 0.2	101 ± 13	6.7	4.4	0.4
J	2.0	1.8 ± 0.3	2.0 ± 0.4	2.2 ± 0.3	2.4 ± 0.5	0.10 ± 0.03	1.1 ± 0.3	282 ± 100	3.9	4.3	0.2
K	2.9	1.5 ± 0.3	< 1.0	1.9 ± 0.3	< 1.4	0.12 ± 0.03	< 0.8	185 ± 58	3.4	4.3	0.2
L	3.0	1.9 ± 0.2	1.6 ± 0.3	2.5 ± 0.3	2.1 ± 0.4	0.19 ± 0.03	0.8 ± 0.2	154 ± 31	4.5	4.3	0.3
M	1.7	2.0 ± 0.2	< 1.0	2.3 ± 0.3	< 1.1	0.27 ± 0.03	< 0.5	117 ± 20	4.1	4.4	0.2
N	2.1	5.1 ± 0.2	1.8 ± 0.3	6.2 ± 0.3	2.2 ± 0.4	0.45 ± 0.03	0.4 ± 0.1	176 ± 15	10.8	4.3	0.6
O	0.5	5.0 ± 0.2	1.7 ± 0.3	5.2 ± 0.2	1.8 ± 0.3	0.55 ± 0.03	0.3 ± 0.1	143 ± 10	9.3	4.3	0.5

Quoted errors are 1σ and limits are 3σ .

^a Measured in a 3 arcsec aperture and corrected for the velocity field (see Section 2.1).

^b Corrected for the extinction listed in column 2 using $A_K/A_V = 0.1$.

^c Observed flux density, measured in a 3 arcsec aperture.

^d Assuming instantaneous star formation.

the alignment of H α , Br γ , $10 \mu\text{m}$, $2 \mu\text{m}$, and CO emission at the ILR.

The radio jet to the North-East extends only 6 arcsec from the nucleus and so has not yet impinged on the ring (Wilson & Ulvestad 1983), but it is interesting to speculate on what effect it may have if this happens. Models such as those proposed by Rees (1989) suggest that once a jet's bow shock has passed, clouds will be subjected to an overpressure of $\sim \mathcal{M}^2$ where \mathcal{M} is the Mach number. From the half-apex angle of the cone which they interpreted as the bow wave generated by the jet's motion, Wilson & Ulvestad (1983) estimated that $\mathcal{M} \gtrsim 3$, sufficient to trigger further star formation.

The ionisation cone from the AGN may have an effect on the environment to the North-East of the nucleus since it extends up to and beyond the ring, and may be assisting the star formation by heating the ISM so that the overpressure helps to crush the clouds. Similar mechanisms have been put forward for jet-induced star formation where the hot plasma behind the shock front overpressures the cloud triggering star formation (eg van Breugel et al. 1985; Best, Longair & Röttgering 1997). We consider whether this mechanism may apply here. When clouds first drift in from the galactic disc, they will probably have temperatures $T \sim 10 \text{ K}$ and average densities $n_e \sim 10^3 \text{ cm}^{-3}$; after some time in the environment of the inner galaxy, they will heat up and perhaps coalesce to form bigger, denser clouds with $T \sim 100 \text{ K}$ and $n_e \sim 10^4 \text{ cm}^{-3}$ (Goldsmith 1987; Genzel 1991). These clouds will have pressures P/k of 10^4 K cm^{-3} and 10^6 K cm^{-3} respectively. Once star formation has commenced H II regions can provide the overpressure to propagate star formation throughout the remaining GMCs. At least some of the gas in the ionisation cone photoionised by the Seyfert nucleus is in a high excitation state. This has been modelled by

a number of authors (Evans & Dopita 1986; Bergeron et al. 1989; Nazarova 1994) to have $T = 3\text{--}5 \times 10^4 \text{ K}$ and $n_e = 0.1\text{--}1 \text{ cm}^{-3}$. The pressure due to this phase is then $P/k \sim 10^4 \text{ K cm}^{-3}$, clearly not high enough to affect the GMCs in the current epoch. On the other hand, the soft X-ray morphology, which is aligned toward the North-East, has been attributed to a nucleus-driven wind with a pressure of $2\text{--}8 \times 10^6 \text{ K cm}^{-3}$ (Wilson et al. 1992). These authors suggest this could confine the narrow-line clouds, and would also be sufficient to provide some overpressure on clouds in parts of the ring, perhaps providing an external stimulus for star formation as required in Section 4

7 THE ROLE OF THE NUCLEUS

Bland-Hawthorn et al. (1997) have proposed a model in which the nuclear continuum luminosity incorporates a big blue bump with a turnover at $\varepsilon_1 = 30 \text{ eV}$

$$L_\varepsilon(\text{photons s}^{-1} \text{ eV}^{-1}) = k_1 \varepsilon^{-2/3} \exp[-\varepsilon/\varepsilon_1]$$

as well as a power-law with slope $\alpha = 1.9$ turning over at $\varepsilon_1 = 100 \text{ keV}$

$$L_\varepsilon(\text{photons s}^{-1} \text{ eV}^{-1}) = k_2 \varepsilon^{-\alpha} \exp[-\varepsilon/\varepsilon_2]$$

(k_1 and k_2 are constants) which add together to make a more realistic quasar spectrum of the form shown in Fig. 2. This luminosity heats grains at the circumnuclear ring which are lying within the ionisation cones. The small grains which can easily be heated to high temperatures would be responsible for the enhanced mid-infrared continuum while the larger grains would re-radiate at longer wavelengths. Their model predicts continuum fluxes over a range of wavelengths from $2\text{--}100 \mu\text{m}$, and was envisaged in order to explain the $10 \mu\text{m}$

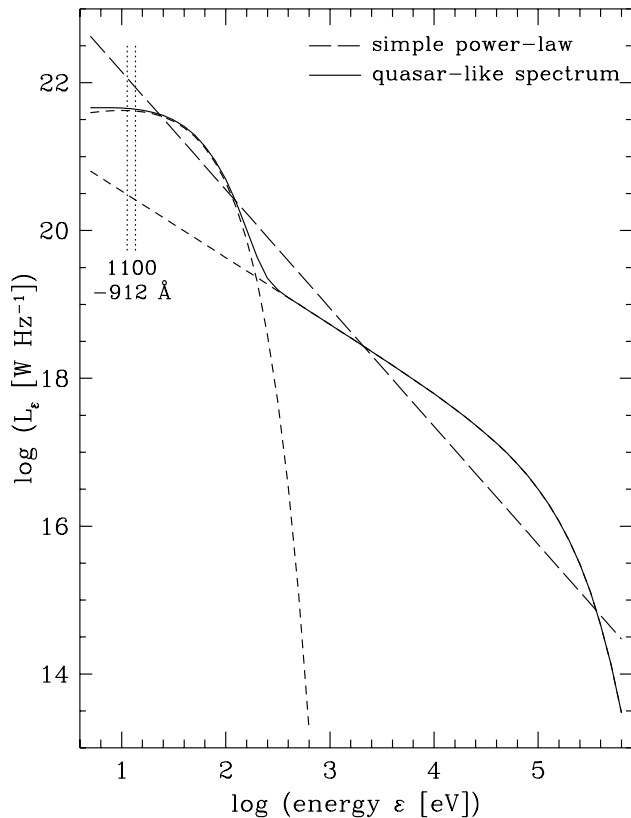


Figure 2. Spectra of the two models of the nuclear luminosity, scaled to the estimated ionising flux of $Q = 8 \times 10^{54} \text{ sec}^{-1}$. That used by Storchi-Bergmann et al. (1992) is a simple power-law, while that from Bland-Hawthorn et al. (1997) has a more realistic quasar form, incorporating a power-law with a turnover as well as a ‘big blue bump’ component.

emission in the ring near the ends of the bar (Telesco & Decher 1988).

In the previous sections we considered only the role of star formation for the emission processes in the ring. But the continuum-residual image (Fig 1) shows that the strongest $2 \mu\text{m}$ emission not associated with the bar coincides almost exactly with the $10 \mu\text{m}$ emission, and hence may be excited by the same mechanism. We are unable to impose any useful constraints on such a model as the predicted total $2 \mu\text{m}$ flux is only 1 mJy, considerably less than that observed at the same positions.

7.1 Circumnuclear H_2 Emission

Fig. 3 shows the alignment of the bar (parallel lines) and the ionisation cone (diverging arrows) with respect to the observed 1-0S(1) emission, although direct interpretation of the figure should be approached cautiously due to the calibration difficulties. The dereddened fluxes in Table 2 show that the intensity of the $\text{Br}\gamma$ flux is similar at both ends of the bar. On the other hand, there is a significant difference in the 1-0S(1) fluxes: that at the North end of the bar is almost twice that at the South end. This is reflected in the S(1)/ $\text{Br}\gamma$ ratio which is 0.7–1.0 to the North and $\lesssim 0.5$ to

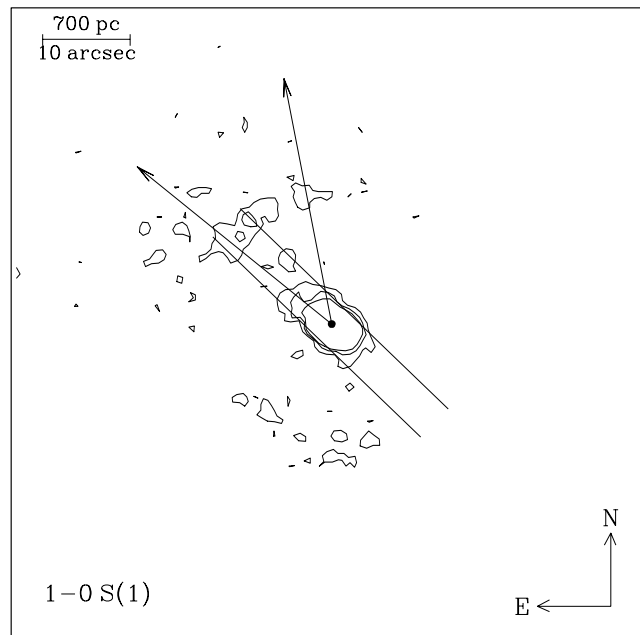


Figure 3. Contour plot of 1-0S(1) in NGC 1068. Contour intervals are as for Fig. 1, and are not corrected for the velocity field. The parallel lines mark the extent of the bar at at 0.5 mJy and position angle 46° . The arrows delineate the extent of the ionisation cone as described by Unger et al. (1992), at PA 11° and PA 51° . The cone extends beyond the ring.

the South. Note that the high S(1)/ $\text{Br}\gamma$ ratios observed in two other regions (J and L) are due to weak $\text{Br}\gamma$ rather than strong 1-0S(1); In every region except A–D the 1-0S(1) flux is less than $2.5 \times 10^{-17} \text{ W m}^{-2}$, while in regions A and B it reaches $3.9 \times 10^{-17} \text{ W m}^{-2}$. We propose that there may be an additional excitation source for the H_2 in these regions.

Puxley, Hawarden & Mountain (1990) proposed the use of the S(1)/ $\text{Br}\gamma$ ratio as a diagnostic for models of star forming regions, assuming that the 1-0S(1) was excited by fluorescence. Their model B, a compact stellar cluster surrounded by a single large H II region, predicts a ratio of 0.1–0.4 for electron densities $\gtrsim 100 \text{ cm}^{-3}$ and photodissociation region gas densities 10^3 – 10^4 cm^{-3} and $N_{\text{UV}} = 10^{51}$ – 10^{52} s^{-1} . Their model A, involving less compact clusters in which each star has its own H II region, produces higher ratios for the same gas densities. However, there is considerable evidence that stars form in compact clusters (eg Meurer et al. 1995), which would tend to result in a low S(1)/ $\text{Br}\gamma$ ratio for purely fluorescent H_2 emission, so that for the ratios observed here fluorescence is unlikely to be the only source of 1-0S(1) flux.

Supernova remnants, appearing in a starburst after 3 Myr, will produce some emission by shocking the ISM; also, where there is such a high density of clouds, shock excitation directly via cloud collisions may also be an important contributor. Together these may explain the observed tendency towards S(1)/ $\text{Br}\gamma \sim 0.5$. However, all the processes mentioned so far will follow either the star cluster or cloud distributions which are fairly uniform around the ring. To account for the large difference in 1-0S(1) flux at opposite ends of the bar, we propose that the extra emission at the North end, 1 – $2 \times 10^{-18} \text{ W m}^{-2}$ in the 3 arcsec apertures, is due to a process unrelated to star formation and

cloud collisions. One possibility is fluorescence at the edges of the molecular clouds by UV radiation from the nucleus. That the nucleus has an important influence on this region is unequivocally demonstrated by the [O III] ionisation cone (Unger et al. 1992). Bergeron et al. (1989) showed that the emission line spectrum in this region could be modelled in terms of photoionisation by soft X-rays from the nucleus. We argue that the UV radiation from the nucleus may also be affecting the line excitation within the molecular clouds in this direction.

In order to quantify this effect, we convert the incident UV flux into an emitted 1-0S(1) intensity, using the detailed models of H₂ excitation from Black & van Dishoeck (1987). These require us to estimate the 912–1100 Å flux, which we can do using the same prescription that Storchi-Bergmann, Mulchaey, & Wilson (1992) used to calculate the luminosity of the torus in NGC 1068. The starting point is the observed characteristics of the ionisation cone, which has a direct line of sight to the nucleus. Then by representing the nuclear continuum emission as a power-law $L_\nu = A\nu^{-\alpha}$, we can derive the coefficient A , and estimate the 912–1100 Å flux incident at the circumnuclear ring (Fig. 2). Storchi-Bergmann et al. calculate the number of ionising photons Q from the ionisation parameter U (from [O III] λ5007/Hβ and [N II] λ6583/Hα) and gas density n (from the ratio of the [S II] lines) measured at several places in the ionisation cone at distances r from the nucleus:

$$Q = U 4\pi r^2 n c$$

The error estimates lead to an uncertainty in nuclear luminosity of a factor of 8, but typical values are $U = 10^{-3}$ and $n = 150 \text{ cm}^3$ at $r = 4 \text{ kpc}$. The coefficient A is found by integrating over all $\nu \geq \nu_0$, where ν_0 is the frequency corresponding to the Lyman limit of 912 Å, giving $A = Q h \alpha \nu_0^\alpha$. The spectral index was measured by Kinney et al. (1991) to be $\alpha = 1.6$, similar to the typical Seyfert 1 value of 1.5. The 912–1100 Å luminosity is simply

$$L_{\text{UV}} = \int_{\nu_1}^{\nu_2} A \nu^{-\alpha} d\nu = Q h \alpha \nu_0^\alpha (\nu_2^{1-\alpha} - \nu_1^{1-\alpha}) / (1 - \alpha)$$

where ν_1 and ν_2 are the frequencies for 1100 and 912 Å respectively. Similarly, integrating over all $\nu \geq \nu_0$ gives the total ionising luminosity as $5 \times 10^{37} \text{ W}$.

Sokolowski, Bland-Hawthorn & Cecil (1991) use a similar method but proceed in the opposite direction: they begin by assuming a luminosity for the nucleus and model the interstellar medium by fitting the observed line profiles. They estimate $10^{-3.1} \leq U \leq 10^{-2.6}$ on the ionisation cone and $10^{-4.5} \leq n \leq 10^{-4.1}$ away from it for $r = 2\text{--}4 \text{ kpc}$, finding it optimal to set $n = 30 \text{ cm}^{-3}$ at 2 kpc, decreasing as r^{-1} . However, their estimate of the nuclear luminosity from X-ray observations does not take account of internal extinction and ignores the possibility of significant flux from photons with $E \gtrsim 15 \text{ keV}$. As such it is about 1/4 that of both the nuclear infrared luminosity (Telesco et al. 1984) and the estimated nuclear bolometric luminosity (Pier et al. 1994). If we corrected for this, the numerical factor would carry through the model and increase their parameter $U \times n$ by a similar amount, making it consistent with that of Storchi-Bergmann et al.

Using the values above, we find $L_{\text{UV}} = 6 \times 10^{36} \text{ W}$. Since there must be rather little extinction in the direction

of the ionisation cone (we assume none) the UV flux incident at the circumnuclear ring, 15.5 arcsec from the nucleus, is $4.4 \times 10^{-4} \text{ W m}^{-2}$, nearly 3 orders of magnitude higher than the mean background in the solar neighbourhood of $6 \times 10^{-7} \text{ W m}^{-2}$ (Black & van Dishoeck 1987). Lastly, if the molecular clouds have densities of $\sim 10^4 \text{ cm}^{-3}$ and we take the covering factor of the clouds to be unity (Planesas et al. 1991 find it to be significantly higher than for Galactic GMCs) then in a 3 arcsec region the models of Black & van Dishoeck give the 1-0S(1) flux as $4 \times 10^{-18} \text{ W m}^{-2}$.

Two important points to consider are: (1) the factor 8 uncertainty from Storchi-Bergmann et al makes little difference in practice as in all cases the UV intensity would still be more than 100 times the background intensity, and the resulting 1-0S(1) line flux would be reduced by at most a factor 2; (2) Sokolowski et al.'s model indicates that the UV intensity away from the ionisation cones is 30 times less than in them, and is insufficient to cause fluorescent H₂ emission.

We also consider whether this scenario is compatible with the quasar-nucleus model of Bland-Hawthorn et al. (1997) described at the beginning of the section. The quasar spectrum they employed, scaled to the same Q that we calculated previously as shown in Fig. 2, results in an ionising luminosity the same as for the simple power law. But the 1100–912 Å luminosity is a factor of 2 less (as the spectrum is essentially flat at these energies), although within the uncertainty of our previous derivation and sufficient to excite 1-0S(1) fluorescence at the ring. In order to explain the $10 \mu\text{m}$ emission, Bland-Hawthorn et al. required an EUV (10 eV – 10 keV) luminosity of $3 \times 10^{38} \text{ W}$, a factor of 6 more than the ionisation and density parameters suggest. However, the resulting 1-0S(1) emission is not significantly enhanced.

We have demonstrated that in principle a nuclear continuum which reproduces the characteristics of the ionisation cone can also cause fluorescence at the circumnuclear ring, and that this mechanism accounts for both the extra flux observed as well as the restricted location.

8 NEAR-NUCLEAR H₂ EMISSION

We include a short section here on the nuclear H₂ emission as our data show, due to considerably lower detection limits and wider field, that the emission is more extended than was previously realised. Hall et al. (1981) found that the emission line spectrum indicated the H₂ was excited thermally with $T_{\text{ex}} \lesssim 2500 \text{ K}$ concluding, as did Oliva & Moorwood (1990), that it should be associated with stellar processes. On the other hand, Rotaciuc et al. (1991) and Maloney (1997) argued that a nonstellar source of ionising radiation such as an X-ray emitting AGN, could be responsible for heating the clouds. Blietz et al. (1994) suggested that there was a close physical connection between the H₂ clouds and radio jet, although the nuclear H₂ knot could not represent the torus proposed by Antonucci & Miller (1985).

Our observations are not of a sufficiently high resolution to shed new light on this debate. However, they do show that weak H₂ emission extends for 10 arcsec (700 pc) along the bar. This is more remarkable because the intensity falls away extremely quickly perpendicular to this axis, more than an order of magnitude in 1 arcsec. Such a morphology is unlikely to arise as a result of collimated emission from

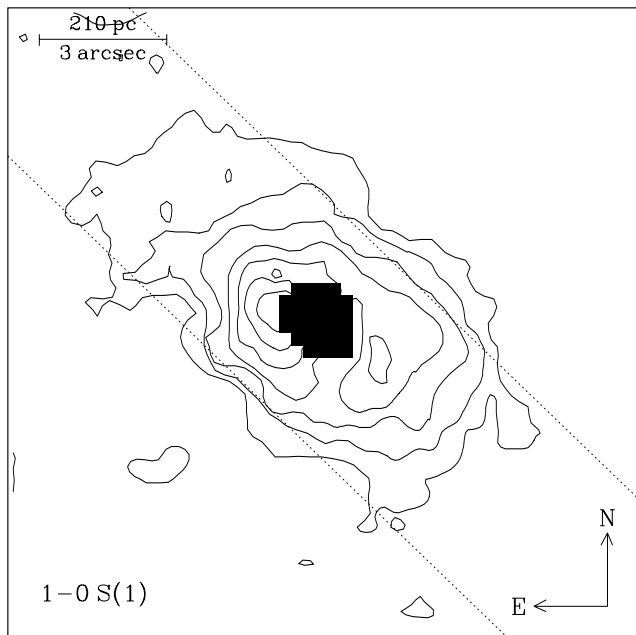


Figure 4. Contour plot of 1-0S(1) in NGC 1068. Contours are from $3.6 \times 10^{-19} \text{ W m}^{-2} \text{ arcsec}^{-2}$ (3.8σ), with levels increasing by a factor of 2, to $229 \times 10^{-19} \text{ W m}^{-2} \text{ arcsec}^{-2}$. These have not been corrected for the 250 km s^{-1} line width. The lowest levels have been smoothed to a resolution of 1.7 arcsec, while the highest levels are at the full resolution of 1.0 arcsec. The parallel dotted lines are the same as those shown in Fig. 3 and delineate the edges of the bar as derived from the 3rd contour in the continuum image. Those pixels near the nucleus which are above some threshold in the on-line image have been blacked out, as these are most affected by saturation.

the nucleus, such as fluorescence due to X-ray irradiation of molecular clouds. This mechanism would only be viable in the directions along which the high energy photons can escape, that is within the ionisation cone. We also consider that star forming processes cannot be responsible as the Br γ flux has a rather different morphology and the S(1)/Br γ ratio is $\gtrsim 1$. Both of these are contrary to expectations of star forming regions.

The alternative we propose is that, since the emitting region appears to coincide with the bar, the excitation mechanism is probably connected with it. The bar inside the circumnuclear ring is a decoupled secondary and typically the co-rotation radius of an inner bar coincides with the ILRs of the primary bar. Helfer (1997) measured the inner rotation curve and found that if corotation occurs at $r = 15 \text{ arcsec}$, the pattern speed is $160 \text{ km s}^{-1} \text{ kpc}^{-1}$, and that there may be inner Lindblad resonances associated with it in the inner hundred parsecs. Consequently, for gas at radii $r < 15 \text{ arcsec}$ inflow can proceed right into the nuclear region. Athanasoulas (1992) discusses the response of gas to barred potentials, showing that shocks occur along the leading edge of a bar where the gas flow is close to radial. These models do qualitatively describe the inner regions of NGC 1068 in which the gas is marginally offset from the bar (to the East of the North-East arm and West of the South-West arm, Helfer 1997), and as such may help in understanding the observed H $_2$ at radii $r < 15 \text{ arcsec}$ which shows weak 1-0S(1) emission along part of the bar, with a morphology entirely consistent

with the CO map. Even though kinematic studies of the inner disc have shown that there may be a general expansion at velocities $50\text{--}100 \text{ km s}^{-1}$ (eg Atherton et al. 1985, Planesas et al. 1991), we do not consider that this would compromise a scenario in which infall is occurring along the bar: clouds form a highly dissipative medium and the loss of angular momentum suffered by clouds in the shock would be sufficient to overcome any reasonable outward accelerating effect, with the relatively high density of clouds in the bar resulting in a net infall. Spatially and velocity resolved observations of HCN (Tacconi et al. 1994) provide further evidence that the bar influences the kinematics of the inner disc, and that gas is streaming along highly elongated orbits. These authors concluded that the H $_2$ in this region was shock excited, and that dissipation was leading to influx to the nucleus at the rate of a few $M_{\odot} \text{ yr}^{-1}$ and a speed of $\sim 50 \text{ km s}^{-1}$.

9 CONCLUSIONS

We have presented the first near-infrared line images of NGC 1068 to include the circumnuclear ring. The fluxes are calibrated to take into account the strong variations in the velocity field across the inner few kpc, which meant that the line flux transmitted by the Fabry-Perot also varied across the image.

We have derived the extinctions in a number of star forming knots by measuring the H α /Br γ recombination line ratios. These are typically in the range $A_V = 1\text{--}3 \text{ mag}$. Comparison of the absolute line fluxes and the continuum due to young stars (obtained by subtracting the underlying elliptical component) to evolutionary synthesis models shows that the star formation in the ring occurred during a short burst within the last 30–40 Myr, and perhaps as recently as 4–7 Myr ago; and that this was the first such episode of star formation in the ring. Although the ionisation cone crosses the North-East segment of the ring, it cannot have a substantial effect on the star formation. On the other hand, the X-ray wind may do so, and once the radio jet reaches the ring it is likely that this will also affect it.

The sizes and masses of the Br γ knots indicate that the stars are forming in compact clusters. The 1-0S(1) fluxes and S(1)/Br γ ratios in these regions suggest some component of the 1-0S(1) emission is due to shock excitation from cloud collisions or supernova remnants. However, there is an excess flux to the North-East, coincident with the region in which the ionisation cone crosses the ring. We have investigated whether this could be due to fluorescence at the edges of molecular clouds by UV radiation from the Seyfert nucleus which is also producing the high excitation lines, and conclude that such a process is possible.

We have found that the nuclear H $_2$ emission is more extended than was previously realised, and that this occurs only along the major axis of the bar. It is possible that this is associated with shocks induced by the streaming motions of clouds along the leading edge of the bar.

ACKNOWLEDGMENTS

We would like to thank staff members at UKIRT for their help in operating the telescope, and Joss Bland-Hawthorn for kindly providing us with his H α image, and as referee for his useful comments and suggestions. This research was supported by a PPARC (EPSRC) research studentship grant.

REFERENCES

- Antonucci R., Miller J., 1985, ApJ, 297, 621
 Atherton P., Reay N., Taylor K., 1985, MNRAS, 216, 17P
 Athanassoula E., 1992, MNRAS, 259, 345
 Bergeron J., Petitjean P., Durret F., 1989, A&A, 213, 61
 Best P., Longair M., Röttgering H., 1997, MNRAS, 286, 785
 Black J., van Dishoeck E., 1987, ApJ, 322, 412
 Bland-Hawthorn J., Sokolowski J., Cecil G., 1991, ApJ, 375, 78
 Bland-Hawthorn J., Voit G., Cecil G., Weisheit J., 1997, Ap&SS, 248, 177
 Blietz M., Cameron M., Drapatz S., Genzel R., Krabbe A., van der Werf P., Sternberg A., Ward M., 1994, ApJ, 421, 92
 Blitz L., 1991, in *The Physics of Star Formation and Early Stellar Evolution*, eds Lada C., Kylafis N., ASI Series vol.342, p.3, Kluwer Academic Publishers, Dordrecht
 Blitz L., Shu F., 1980, ApJ, 238, 148
 Cecil G., Bland J., Tully R., 1990, ApJ, 355, 70
 Evans I., Doptia M., 1986, ApJ, 310, L15
 Gallimore J., Baum S., O’Dea C., 1997, Ap&SS, 248, 253
 Genzel R., 1991, in *The Physics of Star Formation and Early Stellar Evolution*, eds Lada C., Kylafis N., ASI Series vol.342, p.155, Kluwer Academic Publishers, Dordrecht
 Goldsmith P., 1987, in *Interstellar Processes*, eds Hollenbach D., Thronson H., Reidel (Dordrecht), p.51
 Hall D., Kleinmann S., Scoville N., Ridgway S., 1981, ApJ, 248, 898
 Helfer T., 1997, Ap&SS, 248, 51
 Howarth I., 1983, MNRAS, 203, 301
 Keel W., Weedman D., 1978, ApJ, 192, 581
 Kennicutt R., 1989, ApJ, 344, 685
 Kennicutt R., Pogge R., 1990, AJ, 99, 61
 Kinney A., Antonucci R., Ward M., Wilson A., Whittle M., 1991, ApJ, 377, 100
 Leitherer C., Heckman T., 1995, ApJS, 96, 9
 Maloney P., 1997, Ap&SS, 248, 105
 McQuade K., Calzetti D., Kinney A., 1995, ApJS, 97, 331
 Nazarova L., 1994, in *Proc. of the Oxford Torus Workshop*, ed Ward M., University of Oxford, p.31
 Oliva E., Moorwood A., 1990, ApJ, 348, L5
 Osterbrock D., 1989, in *Astrophysics of Gaseous Nebulae and Active Galactic Nuclei*. University Science Books, Mill Valley, USA.
 Pier E., Antonucci R., Hurt T., Kriss G., Krolik J., 1994, ApJ, 428, 124
 Planesas P., Scoville N., Myers S., 1991, ApJ, 369, 364
 Pogge R., 1988, ApJ, 328, 519
 Puxley P., Hawarden T., Mountain C., 1990, ApJ, 364, 77
 Reay N., Atherton P., Walton N., 1986, MNRAS, 218, 13P
 Rees M., 1989, MNRAS, 239, 1P
 Rotaciuc V., Krabbe A., Cameron M., Drapatz S., Genzel R., Sternberg A., Storey J., 1991, ApJ, 370, L23
 Scoville N., Matthews K., Carico D., Sanders D., 1988, ApJ, 327, L61
 Storchi-Bergmann T., Mulchaey J., Wilson A., 1992, ApJ, 395, L73
 Sokolowski J., Bland-Hawthorn J., Cecil C., 1991, ApJ, 375, 583
 Tacconi L., Genzel R., Blietz M., Cameron M., Harris A., Madden S., 1994, ApJ, 426, L77
 Telesco C., Becklin E., Wynn-Williams C., Harper D., 1984, ApJ, 282, 427
 Thatte N., Quirrenbach A., Genzel R., Maiolino R., Tecza M., 1997, ApJ, 490, 238
 Telesco C., Decher R., 1988, ApJ, 334, 573
 Unger S., Lewis J., Pedlar A., Axon D., 1992, MNRAS, 258, 371
 van Breugel W., Filippenko A., Heckman T., Miley G., 1985, ApJ, 293, 83
 Wilson A., Ulvestad J., 1983, ApJ, 275, 8
 Wilson A., Elvis M., Lawrence A., Bland-Hawthorn J., 1992, ApJ, 391, L75
 Young J., Kleinmann S., Allen L., 1988, ApJ, 334, L63

This paper has been produced using the Royal Astronomical Society/Blackwell Science L^AT_EX style file.